Sustainable Structures
ISSN: 2789-3111 (Print); ISSN: 2789-312X (Online)
http://www.sustain-dpl.com/journal/sust
DOI: 10.54113/j.sust.2025.000063

ORIGINAL ARTICLE

Mechanical behavior of additive manufactured wood-based composites for construction

Milinda Yapa Hamillage[a], Robert Carne[b], Armando G McDonald[c], Michael Maughan[b], Ahmed A Ibrahim[a], Daniel J Robertson[b,*]

[a]Department of Civil and Environmental Engineering, University of Idaho, Moscow, Idaho, 83844, United States.
[b]Department of Mechanical Engineering, University of Idaho, Moscow, Idaho 83844, United States.
[c]Forest and Sustainable Products Program, Department of Forest, Rangeland and Fire Sciences, University of Idaho, Moscow, Idaho 83844, United States
[*]Corresponding Author: Daniel J Robertson. Email: danieljr@uidaho.edu

Abstract: Additive manufacturing of composites composed of wood residues and ecofriendly binders such as sodium silicate could reduce the carbon footprint of the construction industry. In this paper the spatially varying mechanical behavior of a single layer of a 3D-printed wood-sodium silicate composite with a 50:50 wt.% known as PrinTimber was investigated. Flexural testing revealed the outer edges of a single printed layer of composite material exhibited greater strength compared to the inner regions of the same sample. Furthermore, tensile tests demonstrated that the longitudinal modulus of elasticity of a single layer was lower than the transverse modulus of elasticity of the same layer. Optical images revealed the 3D printing process tended to arrange wood fibers in a particular manner. The unique fiber arrangement within the layer explains the observed directional dependent response of the sample.

Keywords: PrinTimber, additive manufacturing, wood, sodium silicate, construction

1 Introduction

According to the United Nations Environment Program the built environment sector accounts for 37% of energy related carbon emissions on a global scale [1]. Carbon emissions occur at every stage of a building's life cycle, from the extraction and processing of raw materials, through construction and operation, to deconstruction and disposal. The extent of emissions during the manufacturing and disposal phases depends on the types of materials used. For example, the cement industry alone contributes to as much as 8% of global CO_2 emissions [2]. Integrating environmentally friendly materials and manufacturing methods into construction practices is critical to reducing the carbon footprint.

Advancements in large-scale additive manufacturing, or 3D printing, [3, 4] combined with the use of environmentally friendly materials [5, 6] could significantly improve the sustainability of the construction industry. The application of additive manufacturing in building construction is a relatively recent innovation, with initial demonstrations and theoretical explorations emerging in 2014 [7, 4]. Unfortunately, concrete is the most commonly used material for 3D printing in the construction industry [8]. Using a more sustainable material to 3D print structures presents several advantages. For example, wood is a well-known and highly investigated renewable material. However, only 40% of wood volume

Received: 4 October 2024; Received in revised form: 4 January 2025; Accepted: 28 January 2025

is converted into usable lumber [9]. 3D printing structures from wood residues could reduce cost and lower the carbon footprint.

Extensive research has been done on additive manufacturing of wood composites in small tabletop sized 3D printers [10-12]. However, the application of wood in large-scale additive manufacturing is relatively more scarce [13]. A brief summary of several studies in this area are as follows. Henke and Treml [14] explored large-scale additive manufacturing using spruce wood chips mixed with gypsum, methyl cellulose, sodium silicate, and cement as binding agents. Methyl cellulose and sodium silicate showed poor mechanical performance. In contrast, gypsum and cement provided better results, with cement achieving the best mechanical properties. In a related study, Henke et al. [15] developed an extrusion process for constructing building elements using wood chip concrete, composed of Portland-limestone cement and untreated softwood chips mixed in a 1:1 volumetric ratio.

Gardner et al. [16] 3D printed a boat roof tooling mold, created using a composite material inclusive of 20 wt.% wood flour and 1 wt.% cellulose nanofibrils within a polylactic acid (PLA) matrix. Zhao et al. [17] developed a 3D printing process using poplar fiber-reinforced PLA composites, composed of 20% poplar fibers and 80% PLA by weight, successfully demonstrating the suitability of this material for large-scale additive manufacturing by 3D printing a podium base. Additionally, their findings revealed that the elastic modulus of the composite initially increased and then decreased as the fiber size increased from less than 180 μm to 2360 μm. A PLA-wood based 3D-printed building prototype was constructed through a collaboration between Oak Ridge National Laboratory and the University of Maine, called BioHome3D [18]. The building prototype was printed in four sections and transported to site for assembly.

A project is currently underway at the University of Idaho in collaboration with Auburn University. The project aims to develop the scientific foundation needed to transform minimally processed natural wood waste into 3D-printed houses [19]. A unique aspect of the project is the use of thermoset binders as opposed to thermoplastic binders such as PLA. Using thermoset binders results in lower embodied energy as the material does not need to be heated prior to flowing through an extruder. As part of this project, Orji et al. [20] explored the use of wood fiber and sodium silicate mixtures as a viable material for additive manufacturing, demonstrating promising results in terms of mechanical and thermal properties. Carne et al. [21] utilized the same wood-sodium silicate based composite to design and fabricate a single screw extrusion based 3D printing system, from which the material investigated in this paper was manufactured. This extrusion based 3D printing system which utilizes wood residues and thermoset binders has been named PrinTimber.

Fiber orientation is a critical factor influencing the mechanical properties of composites. The effect of screw extrusion processes on fiber alignment has been studied in materials that employ low concentrations of fiber [22-24]. However, the effect of screw extrusion processes on fiber alignment in materials with a high concentration of wood fiber (like the one being investigated in this study) have not been studied. A lack of understanding of fiber alignment significantly limits our ability to effectively utilize wood-based composites, as it impacts their mechanical properties and swelling and shrinking behavior. Additionally, understanding fiber alignment is essential for exploring the potential of incorporating chopped fibers to reinforce the material. The work presented below provides insights into fiber arrangement, which can serve as a foundation for developing detailed micromechanical models to explain and predict how fiber alignment influences mechanical properties.

Understanding the mechanical behavior of additively manufactured wood based composites that use thermoset binders (PrinTimber) is essential in determining their suitability for 3D printing in construction. This paper therefore investigates the mechanical behavior of a 3D-printed wood-sodium silicate composite, with a focus on the mechanical properties of a single printed layer. The composite's homogeneity, as well as spatially and directionally dependent mechanical properties were studied. Specifically, flexural tests were performed on specimens with different thicknesses to identify the point at which the material began to exhibit continuum behavior. Tests were then conducted to evaluate the mechanical behavior of different regions within a single printed layer. The tensile behavior both along the length of the printed layer and in the transverse direction was evaluated. The effects of the manufacturing process on the macrostructural arrangement of wood particles in the sample was also investigated in relation to mechanical behavior.

2 Methods

2.1 Materials

Wood residue was obtained from the Plummer Forest Products lumber mill in Post Falls, ID and sifted using a 20-mesh screen followed by a 40-mesh screen. The moisture content of the sifted wood residue was between 7.2-7.6 wt.%. The composition of the sawmill residue by type of tree species is shown in **Tab. 1**. A 37 wt.% solution of sodium silicate was obtained from ThermoFisher Scientific, Waltham, MA, USA. A sieve analysis combined with the use of optical microscope images was used to determine particle size and distribution of the sifted wood residues.

Table 1. Weight % of different tree species found in the sawmill residue

Tree Species	Weight %
Douglas-fir	40
Grand-fir and Hemlock	34
Ponderosa and Lodgepole pine	17
Ceder	7
Spruce	2

2.2 Additive Manufacturing Process

Sodium silicate was mixed with sifted wood residue at a 50:50 wt.% ratio on a dry basis. An extrusion-based 3D printing system was used to fabricate test samples as shown in **Fig. 1**, [21]. The wood-sodium silicate mixture was mixed and fed into the funnel where it was guided forward using a constant pitch screw rotating at 40 RPM inside a 35 mm diameter water cooled barrel. At the end of the barrel, the wood sodium silicate mixture was pushed through a die equipped with a pressure transducer. The typical pressure reading at the die was 11 MPa during the sample printing process. The material then traveled through a Teflon lined braided steel hose and a nozzle, both of which had an internal diameter of 22 mm. The nozzle was attached to a 3D printing system composed of an X-Y gantry and a print bed that could be raised and lowered in the Z direction [21]. Samples were produced using a nozzle height of 15 mm from the print bed. A single printed layer is shown in **Fig. 2a**. The 1-axis shown in the figure will be referred to as the longitudinal direction, while 2-axis will be referred to as the through-thickness direction, and the 3-axis will be referred to as the transverse direction. A single printed layer of extrudate measured 15-17 mm in height (through-thickness) and 35-50 mm in width (transverse direction) **Fig. 2b**. After manufacture, samples were dried in an air-conditioned laboratory space. The moisture content of samples ranged between 12% and 14% at the time of testing.

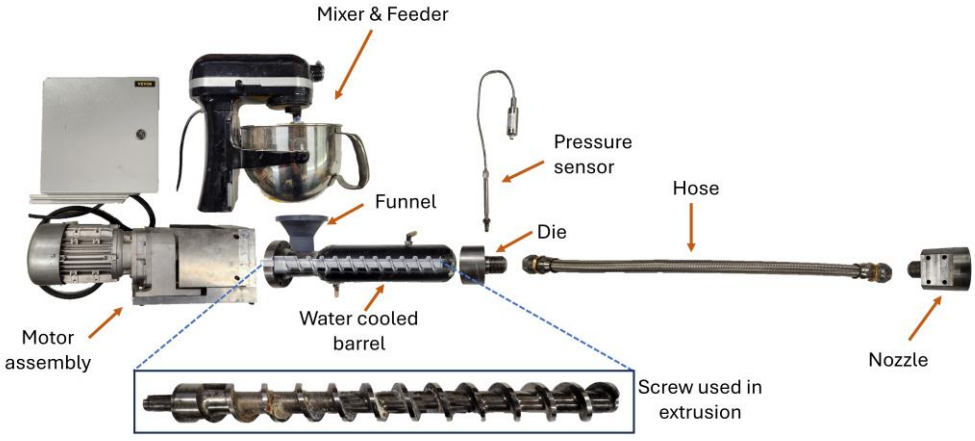

Fig. 1. Components of the printer system used to manufacture the wood-sodium silicate composite.

2.3 Particle orientation of printed samples

It was hypothesized that the additive manufacturing process would preferentially align larger wood particles in certain directions creating sample anisotropy. Optical images were used to determine the spatial orientation and arrangement of wood particles within a single printed layer of wood sodium

silicate. Images were acquired at various stages of the additive manufacturing process and at various sections or planes through the thickness of 3D printed samples.

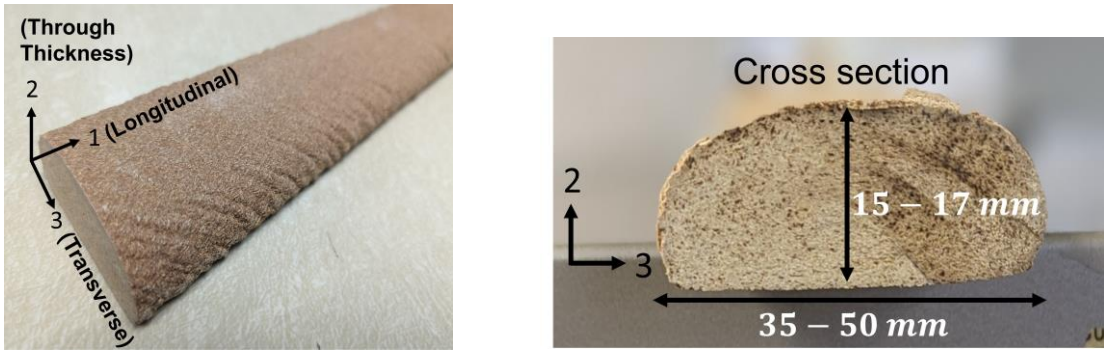

(a) (b)

Fig. 2. (a) Printed wood-sodium silicate composite, (b) cross section of printed wood sodium silicate composite with typical dimensions.

2.4 Evaluating continuum behavior and size effects

Three-point bending experiments were conducted to investigate the effect of specimen size on mechanical property measurements and to determine at what spatial scale a continuum assumption could be made. Specimens were prepared, as illustrated in **Fig. 3a.** Four specimens were tested at thicknesses of 2 mm and 4 mm and six specimens were tested at a thickness of 6 mm. All specimens were obtained from the middle most portion of the same 3D printed sample and were 15 - 16 mm wide. A span-to-thickness ratio of 14 was maintained for all three-point bending experiments (**Fig. 3b**). The tests were performed on a 5944 series Instron universal testing machine with a constant displacement rate of 0.3 mm/min.

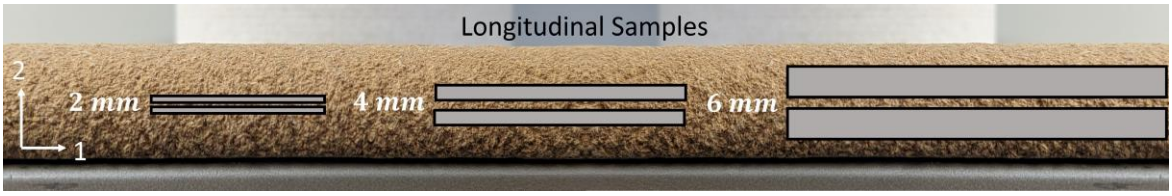

(a)

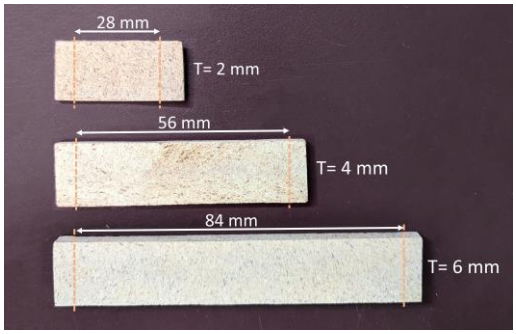

(b) (c)

Fig. 3. (a) Three-point bending specimens with thicknesses of 2 mm, 4 mm and 6 mm extracted from the center most portion of the 3D printer layer. (b) The dimensions of the extracted specimens. (c) The three-point bending test setup.

The apparent flexural modulus of elasticity (E_f) and flexural strength (S_R) were determined by [25],

$$E_f = \frac{PL^3}{4bT^3\Delta} \quad (1)$$

$$S_R = \frac{3p_{\max}L}{2bT^2} \tag{2}$$

where P is the applied load, P_{max} is the maximum load, L is the span, b is the width and T is the thickness of the specimen, and Δ is the cross-head displacement of the Instron testing machine.

2.5 Specimen Preparation

It was determined that test specimens needed to be at least 6 mm thick to ensure continuum behavior (see Section 3.3). This presented a challenge to determine spatial variation in mechanical properties across the thickness because the height of a printed layer is 15-17 mm. Therefore, only two test specimens were produced across the thickness of a 3D printer layer as depicted in **Fig. 4**. A total of twelve specimens were created (i.e., six pairs of specimens).

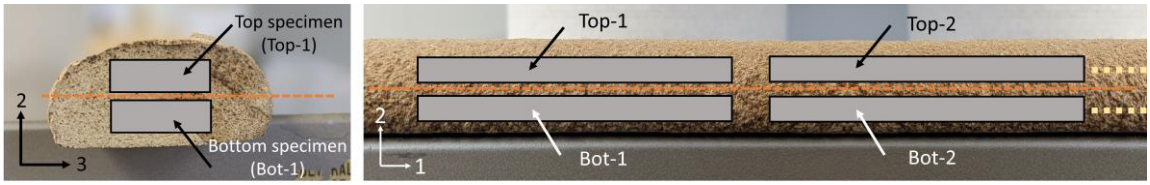

Fig. 4. Three-point bending test specimens. In total, 12 specimens were extracted, six from the top and six from the bottom of the 3D printed layer.

2.6 Spatial variation in flexural modulus and bending strength

Previous studies have concluded that 3D printed wood-sodium silicate composites exhibit much lower tensile strengths than compressive strengths [21]. Therefore, during bending tests, failure always occurs on the tensile side of the specimen. Because of this, test specimens were strategically arranged in pairs to enable fair comparison of differences in strength between the middle of the 3D printed layer and the outer regions of the 3D printed layer. In particular, the Top-1, Top-3 and Top-5 specimens were oriented such that material from the outer region of the 3D printed layer was being loaded in tension while for Top-2, Top-4 and Top-6 specimens the material from the inner region of the 3D printed layer was being loaded in tension. All the 'Bottom' specimens were oriented such that material from the outer region of the printed layer was being loaded in tension. All tests were performed with the same conditions specified in Section 2.4. This arrangement enabled multiple comparisons between specimens to determine the difference in strength both along the length and through the thickness of the sample as described below.

Preliminary testing revealed that the specimen orientation did not affect flexural modulus measurements. In particular, nondestructive bending tests were conducted within the elastic range of three different test specimens. Each test specimen was tested in two orientations. There was no observable difference in flexural behavior based on orientation. Therefore, the flexural moduli of all specimens (Top and Bottom) were plotted to scan for differences in modulus along the length and through the thickness of a single 3D printed layer. To scan for differences in bending strength along the length of a single 3D printed layer, specimens were grouped according to orientation and values were plotted.

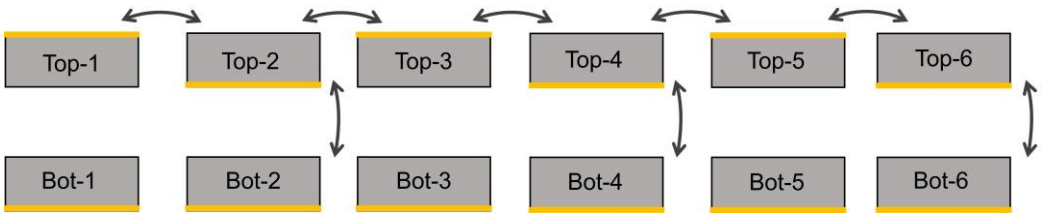

Fig. 5. Specimen pairs for flexural strength evaluation, with arrows indicating paired comparisons. The highlighted surface on each specimen represents the tension region during the 3-point bending test.

In addition, a paired analysis between test specimens was conducted to determine variations in bending strength through the thickness of a single 3D printed layer. In particular, when the top specimen

was tested in a flipped orientation (Top-1, Top-3, and Top-5) it was compared to other Top specimens immediately adjacent to it (Top-2, Top-4, and Top-6) which were in an unflipped orientation. In addition, Top-2, Top-4, and Top-6 specimens were compared to the test specimens immediately below them (Bot-2, Bot-4, and Bot-6). The specimen pairs are illustrated in **Fig. 5**. In this way each pair composed one specimen in which the tensile surface of the specimen contained material from the outer portion of the 3D printed layer while the tensile surface of the other specimen contained material from the inner portion of the 3D printed layer.

2.7 Longitudinal and transverse tensile behavior

Specimens needed to be 6 mm thick to ensure continuum behavior (see Section 3.3). This prevented fabrication of three-point bending specimens in the transverse direction as adequate span to thickness ratios could not be achieved. Therefore, tensile test of dog-bone shaped specimens were used to analyze differences in the longitudinal and transverse properties of the PrinTimber material. Specimen dimensions were established using a scaled-down version of the specimens recommended in ASTM D1037 [26]. Typical specimen dimensions and the experimental set up are shown in **Fig. 7**. The thickness of the test specimens ranged from 6 to 7 mm. An Epsilon extensometer (model 3442) with a 10 mm gauge length was used to measure strain during the test. All tests were conducted on an Instron universal testing machine with a displacement rate of 0.4 mm/min until failure. To determine differences in transverse and longitudinal properties a paired analysis was conducted similar to the one outlined Section 2.5. In particular, specimens were prepared as shown in **Fig. 6**. A total of 12 longitudinal specimens and 12 transverse specimens were produced. The properties of each specimen were compared to the properties of those specimens immediately adjacent to it. For example, T2 was compared to L1 and L2.

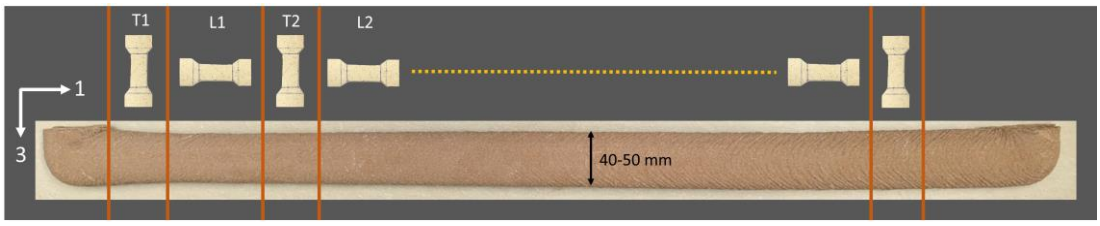

Fig. 6. Selection of paired transverse (T) and longitudinal (L) specimens.

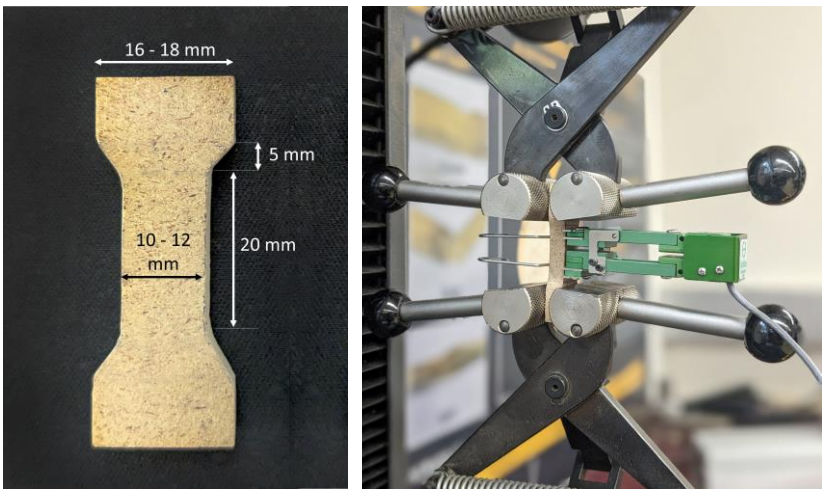

(a) (b)

Fig. 7. (a) Dimensions of tensile test specimens. (b) Test setup with a tensile specimen clamped in self-tightening grips and an extensometer in place.

3. Results and discussion

3.1 Sieve analysis results and particle characterization

Results from the sieve analysis used to characterize particle size and particle distribution of the sifted wood residues are shown in **Fig. 8a**. Results indicated 53% of the wood particles by weight had a particle size greater than 420 μm, whereas 27% of the wood particles were between 420 μm -250 μm and 20% of particles were less than 250 μm. A significant portion of the particles over 420 μm had an elongated shape. These elongated particles are expected to play a dominant role in determining mechanical properties. Therefore, 140 particles with lengths greater than 1 mm were separated and measured using optical images taken from an AM scope optical microscope. Their length distribution is presented in **Fig. 8b**. Of the 140 particles, 34% were 1.5-2 mm long, 28% were 2-2.5 mm long and 7% were 3-3.5 mm long. None of the fibers were longer than 3.5 mm.

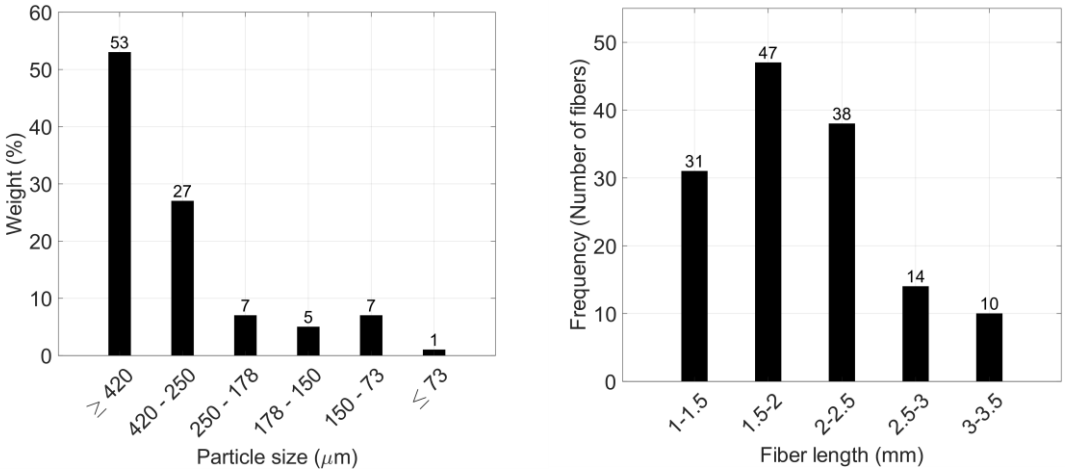

(a) (b)

Fig. 8. (a) The sieve analysis results of sifted wood residues (b) Distribution of fibers with lengths ≥ 1 mm.

3.2 Particle orientation within the printed layer

Fig. 9a and **Fig. 9b** display cross-sectional images of the wood-sodium silicate extrudate after exiting from the print nozzle (but before being deposited on the print bed). The wood particles are oriented in a spiral configuration (due to the rotating screw).

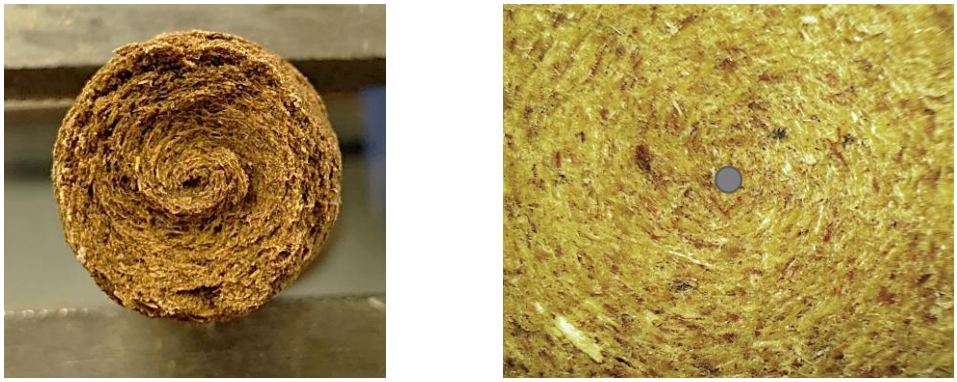

(a) (b)

Fig. 9. (a) Cross-sectional view of the highly compressed wood-sodium silicate mixture upon extrusion from the nozzle. (b) Magnified optical micrograph of cross section of the extrudate exiting from the nozzle with the center denoted by the gray circle.

After the extrudate exits the nozzle, it is deposited onto the print bed which is oriented perpendicular to the nozzle as shown in **Fig. 10a**. Upon deposition, the material at the back of the nozzle is pushed back which creates the ripples seen in **Fig. 10b**. In contrast, the material at the front of the nozzle is pushed in the print direction and gets deposited at the bottom of the layer.

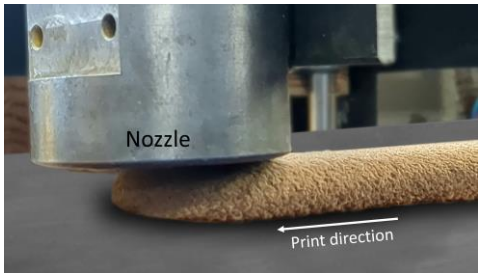

(a)

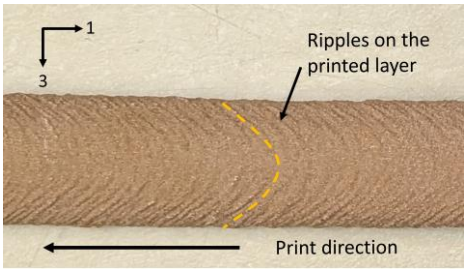

(b)

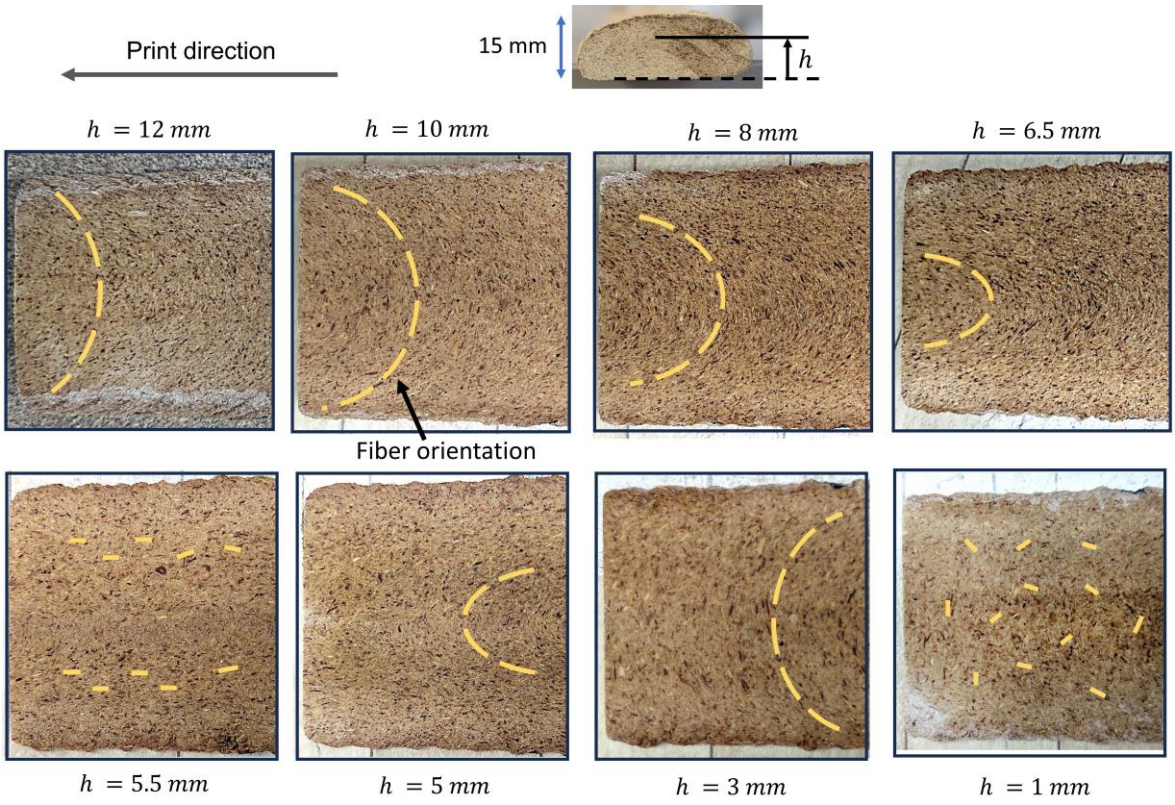

(c)

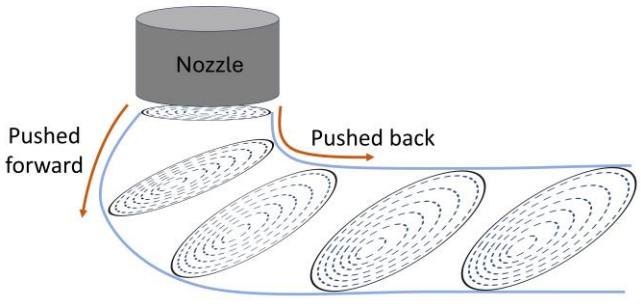

(d)

Fig. 10. (a) The wood-sodium silicate mixture as it is extruded from the nozzle. (b) Plan view of the printed wood-sodium silicate composite layer with the ripples that occur due to material push back at the back of the nozzle. (c) Fiber arrangement at different heights of a 15 mm thick printed layer. '***h***' is measured from the bottom of the layer. (d) General schematic representation of fiber arrangement and flow mechanisms during material deposition.

To determine the effects of printing on the particle arrangement, images were acquired at different

heights in the through-thickness direction of a 15 mm thick printed layer, as shown in **Fig. 10c**. At the top of the sample (h = 15 mm) the elongated fibers follow the path of the ripple shown in **Fig. 10b**. In the range h = 12 mm to h = 6.5 mm the fiber orientation is well defined and is curved opposite to the print direction following the same pattern as the ripples seen in 10b. It can be seen that the degree of curvature of the orientation path of the elongated particles tends to increase as the height decreases. At h = 10 mm and h = 8 mm a small band of fibers can be seen near the edges of the sample that are fully oriented in the print direction. This band increases in size as height decreases to h = 6.5 mm with more elongated particles being oriented in the print direction. At height h = 5.5 mm most of the fibers are oriented parallel to the print direction. Between h=5.5 mm and h = 5 mm, fibers begin to curve in the print direction (opposite the direction of the ripples seen on the top of the sample). This is due to material exiting the front of the nozzle being pushed in the print direction. A random fiber orientation is seen at h = 1 mm which could be due to unrestricted material flow in the outer regions. In summary, at the top of the sample, elongated particles follow the path of the ripples shown in **Fig. 10b** whereas near the bottom of the sample the elongated particles follow a path that is almost a mirror image of the path at the top of the sample. In the middle of the sample exists a transition region in which the particle orientation gradually shifts. However, the middle of this transition does not occur in the middle of the sample but rather appears to occur at about one third of the height of the 3D printed layer. Thus, test specimens that are obtained from the top two thirds of the sample predominantly contain elongated particles oriented in a curved path opposite to the print direction whereas specimens obtained from the bottom one third of the 3D printed layer predominantly contain elongated particles orientated in a curved path in the print direction (**Fig. 10d**).

3.3 Continuum behavior and size effect results

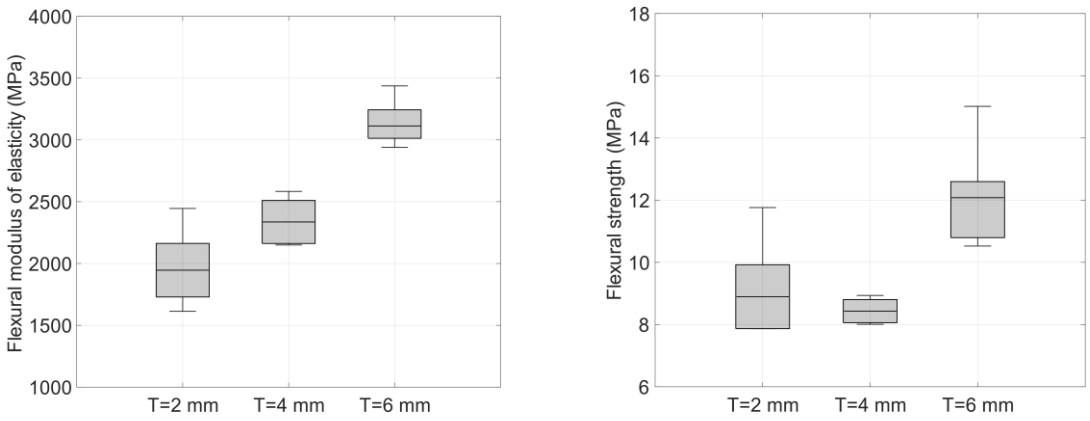

(a) (b)

Fig. 11. Boxplot showing (a) the flexural modulus and (b) the flexural strength of specimens with thicknesses (T) of 2 mm, 4 mm, and 6 mm. The horizontal line within each box represents the mean value. The error bars extend to the minimum and maximum data points.

The effect of specimen thickness on mechanical properties was evaluated by conducting three-point bending flexural tests on specimens of varying thickness but identical span to thickness ratios. As illustrated in **Fig. 11a,** the flexural modulus increased as the specimen thickness increased. On average, the 4 mm and 2 mm thick specimens exhibited a 25% and 37% reduction in flexural modulus, respectively, compared to the 6 mm specimens. The flexural modulus values of the 6 mm thick specimens showed good correlation with flexural test of entire printed layers (15-17 mm thick) [21]. The authors therefore concluded that if the minimum dimension of the specimens is at least 6 mm thick, then the material will act as a continuum. This parameter is primarily influenced by the long wood fibers present in the composite. If specimens are created with lower thicknesses, then these long fibers that provide additional reinforcement may be cut off, thus reducing the overall stiffness of the specimen. Results from the sieve analysis of the wood particles demonstrated that the longest wood particles were on the order of 3.5 mm in length. Thus, the material may begin to exhibit continuum behavior at a

thickness less than 6 mm (potentially occurring anywhere between 4 and 6 mm). However, for the remaining mechanical experiments, 6 mm was used as the minimum baseline.

The effect of specimen thickness on flexural strength was also investigated. **Fig. 11b** shows the flexural strength of 2 mm, 4 mm and 6mm thick specimens. In all the tests, failure was initiated on the side of the specimen being loaded in tension. On average, the flexural strength of the 6 mm thick specimens was 35-44% higher compared to the 2 mm and 4 mm thick specimens. Strength is influenced by various factors. In the wood composite under investigation, it is governed by the properties of constituents (sodium silicate and wood fiber), the size and distribution of wood particles within the composite, the bonding between larger elongated particles and the surrounding sodium silicate and finer wood particulates, as well as any defects arising from the manufacturing process. In the 2 mm thick specimens, the probability of the presence of critical material defects is low compared to the 4 mm and 6 mm thick specimens simply because there is less cross-sectional area in the thinner specimen. However, the thinner specimens may also have a lower probability of containing longer wood particles that are believed to provide reinforcement against tensile failure. In other words, bending strength is determined by various parameters that can interact or counteract each other in non-intuitive ways.

3.4 Spatial variation of flexural modulus

Flexural modulus values of all specimens are plotted in **Fig. 12**. The average flexural moduli of specimens obtained from the top and bottom of the 3D printed layer were 3168 MPa and 3272 MPa respectively. In general, there is no significant difference in flexural stiffness between the top and bottom of the 3D-printed layer.

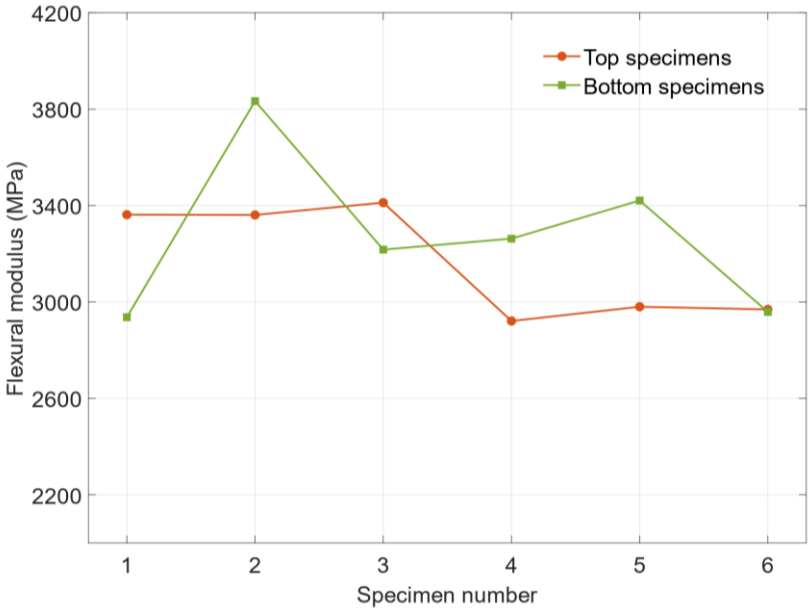

Fig. 12. The variation of the flexural modulus along the printed wood-sodium silicate composite layer at upper and lower regions.

3.5 Spatial variation of bending strength

The flexural strengths of all specimens are shown in **Fig. 13a**. The flexural strength of specimens varies along the length of the 3D printed layer. This was expected and is due to natural variation in wood residue and the manufacturing process. Results from the paired analyses explained in the methods section are shown in **Fig. 13b**. This figure compares the strength of outer regions of the 3D printed layer to the strength of the inner regions of the 3D printed layer. On average, the outer portions of the 3D printed layer were 18% stronger than the inner regions of the sample. This may be because, during the manufacturing process, the wood-sodium silicate mixture is first compressed along the outer edges as it moves forward through the barrel. The middle or center portion of the extrudate is filled last after the shank of the screw is reduced. This may create a less dense and weaker region in the middle of the 3D

printed layer. It is also possible that curing dynamics may play a role and that the outer portions of the sample may dry/cure at a different rate than the inner regions.

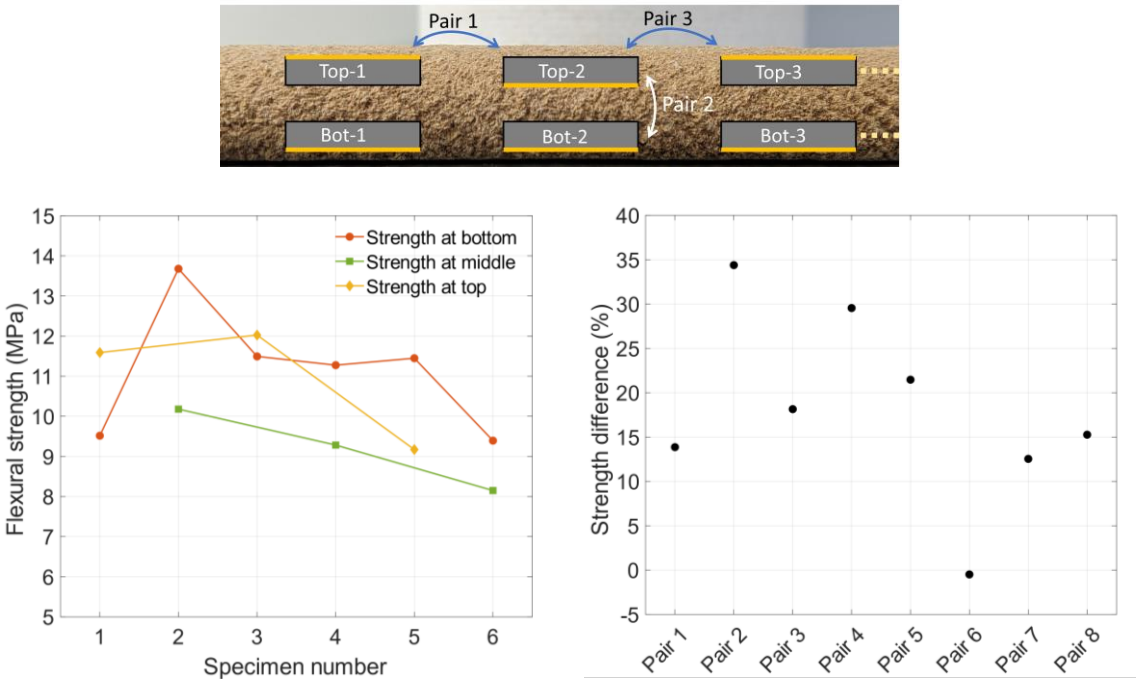

Fig. 13. The first three sets of flexural test specimens are displayed, with the colored line indicating the tensile surface during the 3-point bend test. (a) Flexural strength at the bottom, middle and top regions of the 3D printed layer. (b) The percent difference in flexural strength of the outer region compared to the inner region of the 3D printed layer.

3.6 Longitudinal and transverse tensile behaviors

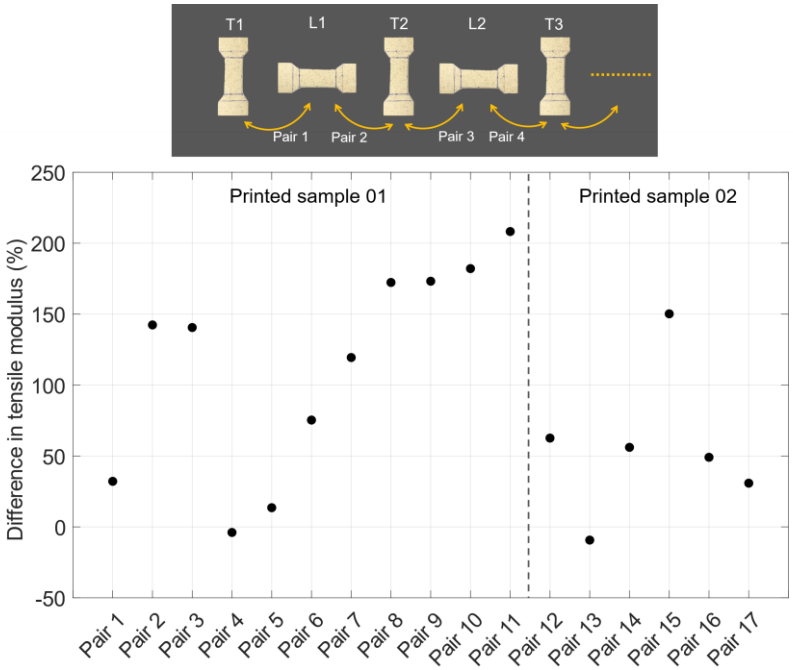

Fig. 14. Percentage difference in tensile modulus of the transverse specimens compared to longitudinal specimens. On average the transverse specimens were twice as stiff as the longitudinal specimens.

To determine differences in longitudinal modulus and strength VS transverse modulus and strength,

dog-bone shaped specimens were created and subjected to tensile tests. The difference in tensile modulus in the longitudinal and transverse directions is shown in **Fig. 14**.

The dotted line in the figure separates specimen sets obtained from two different 3D printed samples. The figure indicates that on average the transverse tensile modulus is about twice as large as the longitudinal tensile modulus. The observed difference in longitudinal and transverse moduli of the specimens can be attributed to the arrangement of elongated wood particles in the 3D printed layer. In particular, all specimens used in this analysis were acquired from the center most portion of the 3D printed layer. The optical images of **Fig. 10c** demonstrate that elongated wood particles are oriented in the transverse direction near the center of the 3D printed layer. Thus, in the transverse specimens the elongated particles were oriented along the direction the load was being applied. Conversely in the longitudinal specimens, the load was being applied perpendicular to the direction of the elongated wood particles.

The ultimate tensile strengths of the transverse and longitudinal direction specimens are presented in **Fig. 15**. The dotted line separates specimen sets obtained from two different 3D printed wood-sodium silicate samples. In general, the results are inconclusive. It appears the strength changes along the length of the 3D printed layer as expected. However, there is no clear trend evident in differences between longitudinal VS transverse strength. This is interesting as there were very clear differences in tensile moduli between transverse and longitudinal specimens. It is important to consider the failure patterns observed in the specimens when interpreting these results.

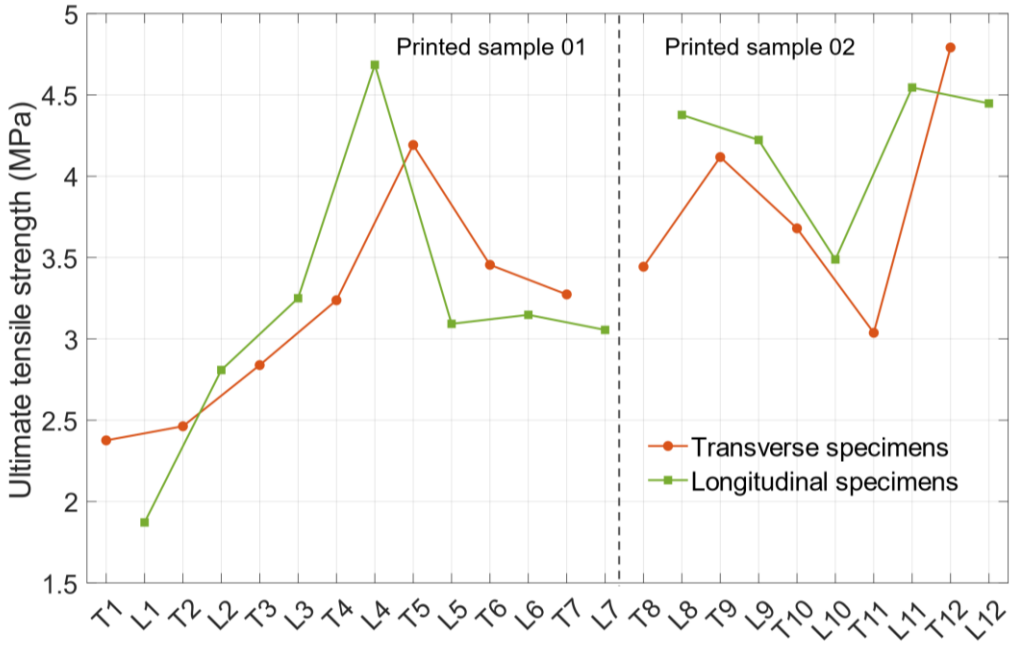

Fig. 15. The variation of ultimate tensile strength of transverse and longitudinal specimens along the printed wood composite layer. Sample 01 and Sample 02 refer to two distinct layers.

Failure patterns of the dog-bone shaped specimens are shown in **Fig. 16**. All of the longitudinal specimens failed near their centers, while all the transverse specimens exhibited failure away from the center. The use of dog-bone shaped specimens is prescribed in numerous testing standards with the goal of ensuring failure occurs near the center of the specimen in the region of constant width. When failure occurs outside of this region (as it did in the present study) the calculated strength values are likely less than the true material strength. This is because stress concentrations exist near the end of the specimen where the width of the specimen necks down. In this study the transverse specimens likely failed away from the center due to the effects of elongated wood particles orientation. The dotted lines in **Fig. 16** show the orientation of the elongated wood particles. In the longitudinal specimens, the wood particles are aligned in a relatively uniform structure, leading to consistent material behavior along the entire length of the specimen. Consequently, failure was observed in the middle region of the specimen, as desired, where the tensile stress is the highest. In contrast, within the middle region of the transverse

specimens, the long fibers are aligned along the loading direction. This likely improves the strength characteristics in the middle region of transverse specimens. However, failure did not occur in this region. Rather failure occurred near the end of the specimen where the wood particles are aligned in a weaker orientation, at an angle to the loading axis. Unfortunately, the shape and size of the dog-bone specimens are limited by the dimensions of the 3D printed layer. This prevented manufacture of other dog-bone shaped specimens that would better ensure failure in the proper region of the transverse specimens. The next step is to better understand the stress distributions within a single 3D printed layer of PrinTimber material by creating a micro-mechanical finite element model that is able to account for the continuously varying distribution of elongated wood fibers within the material.

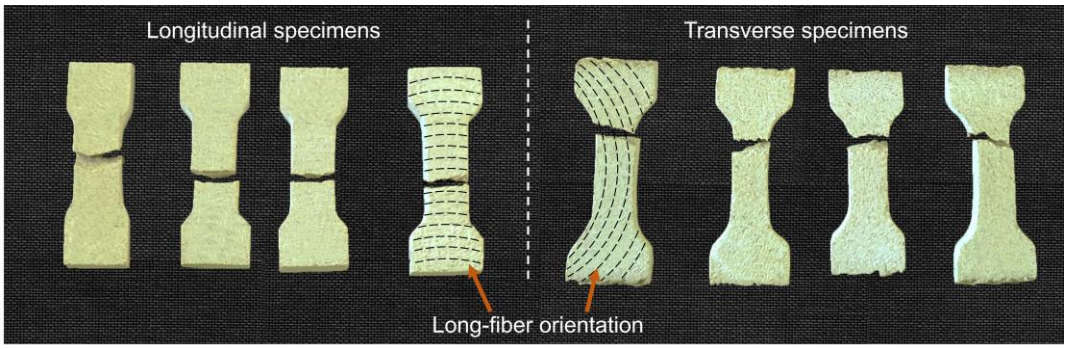

Fig. 16. Longitudinal and transverse specimens after ultimate failure. The dotted lines indicate fiber orientation of the specimens.

4. Conclusions

The flexural and tensile behaviors of a 3D-printed wood-sodium silicate composite were determined. The composite features a complex material structure, characterized by a range of wood particle sizes and orientations. The presence of elongated wood particles (greater than 1mm in length) plays a significant role in determining mechanical properties. The arrangement of these particles is primarily influenced by two key steps in the manufacturing process. First, as the material is pushed forward through the barrel by the rotating screw the particles get oriented into a circular path. Second, as the material is deposited onto the print bed the particle orientation gets altered. In the top region of the 3D printed layer, the particles follow a path which curves away from the print direction. At the bottom of the sample, the particles follow a path which curves in the same direction as the print direction.

Flexural experiments demonstrated that the wood-sodium silicate composite material exhibits continuum behavior at a specimen thickness of 6 mm, with a significant increase in flexural modulus and strength compared to thinner specimens. The spatial variation in the flexural modulus at the upper and lower regions of the printed layer exhibited similar trends. The flexural strength at the center of the printed layer was notably lower compared to the outer edges.

Tensile tests revealed the transverse tensile modulus is about twice as high as the longitudinal modulus. A more comprehensive characterization of the 3D printed wood-sodium silicate composite from experiments is challenging due to the complexity of the spatially varying orientation of wood particles within the sample. Future research focused on developing micro-mechanical finite element models may provide further insight into the bulk behavior of PrinTimber. The experimental data obtained in this study can aid in the development of such models. Further research is also needed to evaluate the mechanical behavior of multilayered wood-sodium silicate composites.

Acknowledgements

The authors wish to acknowledge Yi Wang from Plummer Forest Products for providing wood residues.

Funding Statement

The research work presented in the paper is supported by funding from National Science

Foundation (grant #2119809).

CRediT authorship contribution statement

Milinda Yapa Hamillage: Conceptualization, Methodology, Formal analysis, Investigation, Data Curation, Writing - Original Draft, Writing - Review & Editing, Visualization. **Robert Carne**: Methodology, Investigation. **Armando G McDonald**: Conceptualization, Resources, Writing - Review & Editing, Supervision, Project administration, Funding acquisition. **Michael Maughan**: Conceptualization, Resources, Writing - Review & Editing, Supervision, Project administration, Funding acquisition. **Ahmed A Ibrahim**: Conceptualization, Methodology, Writing – Original Draft, Writing - Review & Editing, Supervision, Project administration, Funding acquisition. **Daniel J Robertson**: Conceptualization, Methodology, Writing – Original Draft, Writing - Review & Editing, Supervision, Project administration, Funding acquisition.

Conflicts of Interest

The authors declare that they have no conflicts of interest to report regarding the present study.

Data Availability Statement

Some or all data, models, or codes that support the findings of this study are available from the corresponding author upon reasonable request.

References

[1] United Nations Environment Program. Building materials and the climate: Constructing a new future. Nairobi 2023.

[2] Andrew RM. Global CO2 emissions from cement production. Earth System Science Data 2018; 10(1): 195–217. https://doi.org/10.5194/essd-10-195-2018.

[3] Ngo TD, Kashani A, Imbalzano G, Nguyen KT, Hui D. Additive manufacturing (3D printing): A review of materials, methods, applications and challenges. Composites Part B: Engineering 2018; 143: 172–196. https://doi.org/10.1016/j.compositesb.2018.02.012.

[4] Wu P, Wang J, Wang X. A critical review of the use of 3D printing in the construction industry. Automation in Construction 2016; 68: 21–31. https://doi.org/10.1016/j.autcon.2016.04.005.

[5] Moretti M. Wasp in the edge of 3D printing, in: 3D Printing for Construction with Alternative Materials, Springer 2023; 57–65. https://doi.org/10.1007/978-3-031-09319-7_3.

[6] Pungercar V, Hutz M, Musso F. 3D print with salt, in: 3D Printing for Construction with Alternative Materials, Springer 2023; 91–125. https://doi.org/10.1007/978-3-031-09319-7_5.

[7] Hager I, Golonka A, Putanowicz R. 3D printing of buildings and building components as the future of sustainable construction? Procedia Engineering 2016; 151: 292–299. https://doi.org/10.1016/j.pro eng.2016 .07.357.

[8] Grand View Research. 3D printing construction market size, share & trends analysis report by construction method (extrusion, powder bonding), by material type (concrete, metal), by end-user (building, infrastructure), and segment forecasts, 2023–2030. https://www.grandviewresearch.com/industry-analysis/3d-printing-construction-market, 2023.

[9] Bell G. Factors influencing the manufacture of sawlogs into lumber in eastern Canada 1951.

[10] Wimmer R, Steyrer B, Woess J, Koddenberg T, Mundigler N. 3D printing and wood. Pro Ligno 2015; 11(4): 144–149.

[11] Das AK, Agar DA, Rudolfsson M, Larsson SH. A review on wood powders in 3D printing: Processes, properties and potential applications. Journal of Materials Research and Technology 2021; 15: 241–255. https://doi.org/10.1016/j.jmrt.2021.07.110.

[12] Khan MZ, Srivastava SK, Gupta M. A state-of-the-art review on particulate wood polymer composites: Processing, properties and applications. Polymer Testing 2020; 89: 106721. https://doi.org/10.1016/j. polym ertesting.2020.106721.

[13] Henke K, Talke D, Buschmann B. Einsatz von Holz bei der additiven Fertigung im Bauwesen: Use of wood in additive manufacturing in construction, in: Proceedings of the 17th Rapid.Tech 3D Conference, Erfurt, Germany, 22–23 June 2021, Carl Hanser Verlag GmbH Co KG 2021; 177.

[14] Henke K, Treml S. Wood-based bulk material in 3D printing processes for applications in construction. European Journal of Wood and Wood Products 2013; 71: 139–141. https://doi.org/10.1007/s00107-0120658-

z.
[15] Henke K, Talke D, Winter S. Additive manufacturing of building elements by extrusion of wood concrete, in: World Conference on Timber Engineering (WCTE 2016), 2016; 2593–2601.
[16] Gardner D, Anderson J, Tekinalp H, Ozcan S, Sauerbier P. Lignocellulosic-filled polymer feedstocks for large scale additive manufacturing of low cost composites, in: Proceedings of the International Forest Products Congress, 2018; 12–22.
[17] Zhao X, Tekinalp H, Meng X, Ker D, Benson B, Pu Y, Ragauskas AJ, Wang Y, Li K, Webb E. Poplar as biofiber reinforcement in composites for large-scale 3D printing. ACS Applied BioMaterials 2019; 2(10): 4557–4570. https://doi.org/10.1021/acsabm.9b00675.
[18] Ferrini-Mundy J, Varahramyan K. 2022 research report: R1 global impact-local relevance, University of Maine, Orono, ME, USA, 2023.
[19] University of Idaho and Auburn University. Printimber project. https://printimber.org/.
[20] Orji BO, Thie C, Baker K, Maughan MR, McDonald AG. Wood fiber-sodium silicate mixtures for additive manufacturing of composite materials. European Journal of Wood and Wood Products 2023; 81(1): 45–58. https://doi.org/10.1007/s00107-022-01861-z.
[21] Carne RH, Alade AA, Orji BO, Ibrahim A, McDonald AG, Maughan MR. A screw extrusion-based system for additive manufacturing of wood sodium silicate thermoset composites. Advances in Mechanical Engineering 2023; 15(11). https://doi.org/10.1177/16878132231210373.
[22] Wang Z, Smith DE. Numerical analysis of screw swirling effects on fiber orientation in large area additive manufacturing polymer composite deposition. Composites Part B: Engineering 2019; 177: 107284. https://doi.org/10.1016/j.compositesb.2019.107284.
[23] Grande C, Torres F. Investigation of fiber organization and damage during single screw extrusion of natural fiber reinforced thermoplastics. Advances in Polymer Technology: Journal of the Polymer Processing Institute 2005; 24(2): 145–156. https://doi.org/10.1002/adv.20037.
[24] Russell T, Heller B, Jack DA, Smith DE. Prediction of the fiber orientation state and the resulting structural and thermal properties of fiber reinforced additive manufactured composites fabricated using the big area additive manufacturing process. Journal of Composites Science 2018; 2(2): 26. https://doi.org/10.3390/jcs2020026.
[25] ASTM D198-05. Standard Test Methods of Static Tests of Lumber in Structural Sizes, 2017.
[26] ASTM D1037-21. Standard test methods for evaluating properties of wood-base fiber and particle panel materials, 2021.